Fine structure on flat surfaces of quasicrystalline Al-Pd-Mn

Z. Shen, C. R. Stoldt, C. J. Jenks, T. A. Lograsso, and P. A. Thiel
Department of Chemistry, Department of Materials Science and Engineering, and the Ames Laboratory, Iowa State University, Ames, Iowa 50011
(Received 13 May 1999)

We have analyzed the fine structure revealed by scanning tunneling microscopy for a flat (within 0.8 Å) fivefold surface of *i*-Al-Pd-Mn. Even though features in the image appear to be arranged randomly, self-similar features are separated by distinct distances. The distribution of such distances is compatible with the separations between pseudo-Mackay icosahedra tangent to the topmost layer, and with separations between other cluster-based units. We propose that the fine structure is due to electronic structure imposed by the clusters. [S0163-1829(99)01035-8]

I. INTRODUCTION

Quasicrystals, discovered in 1982 by Shechtman,[1] are typically binary and ternary intermetallics, often containing 60 to 70 atomic percent aluminum. The bulk structure is remarkable, in that it lacks periodicity but is nonetheless well ordered. Furthermore, it typically exhibits a rotational symmetry element that is crystallographically forbidden, e.g., a fivefold axis.[2,3]

The surface properties of quasicrystals have excited special interest recently.[4] The essential question is, how are the unusual surface properties—most prominently low-surface energy and low coefficient of friction[5]—related to the unusual bulk structure? This broad question soon engenders more specific ones, such as whether the bulk quasicrystalline structure is maintained up to the surface? And which conditions of preparation produce a surface that is thermodynamically stable? The most fundamental answers are obtained by studying clean surfaces. Since surfaces of the Al-rich alloys oxidize readily, such studies must be carried out in ultrahigh vacuum (UHV).

The two main candidates for surface preparation in UHV are currently fracture,[6,7] and ion sputtering with annealing.[8] These two methods produce much different surface morphologies, at least for the icosahedral (*i*) phase of Al-Pd-Mn. Scanning tunneling microscopy (STM) reveals a rough, clusterlike structure after fracture, with surface corrugation on the order of 10 Å,[6] whereas a terrace-step topography exists after sputter annealing, with terrace corrugation on the order of 1 Å or less.[9–12] For the fracture surfaces, the smallest clusters (~10 Å in diameter) have been interpreted as the basic building block of the *i*-Al-Pd-Mn quasicrystal. In one model,[13–16] this structural unit is the pseudo-Mackay icosahedron (PMI). It has been proposed that the fracture front skirts around these clusters (and also around some larger, self-similar aggregates) because of their special stability, leaving them exposed at the surface.[6] Such a model is consistent with the corrugation observed after fracture.

For the sputter-annealed surfaces of *i*-Al-Pd-Mn, cluster structures have also been observed after sputtering.[9–12] Upon annealing, however, the surfaces usually evolve toward a terrace-step topography, with terrace corrugation on the order of 1 Å or less.[9–12] The terraces exhibit intriguing fine structure, although its origin has not been identified. This general type of fine structure was first reported for *i*-Al-Pd-Mn by Schaub, *et al.*[9,10] There has been speculation about the identity of individual features, particularly the dark ''holes,'' which often show local fivefold symmetry.[9,10] It has been suggested that these represent specific types of atoms in the surface, e.g., Mn surrounded by Al-Pd pentagons.[17] It has also been suggested[18,19] that these may represent parts of the Bergman cluster, which is a structural unit emphasized in other structural models.[20,21]

The present paper elucidates the discussion of the terrace fine structure. Following the approach of Schaub *et al.*,[9,10] we examine three aspects of the STM image: its rotational symmetry, its degree of positional order, and the characteristic distances separating individual features. The result from the present paper is that the last aspect, the distribution of characteristic distances, is compared quantitatively with predictions of surface atomic structure based upon a combination of bulk and surface analyses.

II. EXPERIMENTAL DESCRIPTION

STM experiments were performed in an ultrahigh vacuum chamber equipped with an Omicron room temperature STM, Omicron SPA-LEED (spot profile analysis-low energy electron diffraction) system, Auger electron spectrometer, mass spectrometer, and ion bombardment gun. The SPA-LEED achieves high resolution in reciprocal space, with a nominal instrumental limit of about 1200 Å. The base pressure of the chamber is 3 to 4×10^{-11} Torr. The pressure during STM measurements is 4 to 6×10^{-11} Torr. Other papers[8,22] describe our methods of quasicrystalline sample preparation outside UHV. Our method of surface preparation within UHV involves ion bombardment at room temperature and annealing. The sample is sputtered for 15 min each time (1 keV, 12–15 μA sample current without bias). Annealing a fresh sample begins at 400 K, and goes up by 50 K whenever annealing at a given temperature no longer reveals significant surface segregation of carbon and oxygen (although overlap between C and Pd transitions in Auger electron spectroscopy makes it difficult to detect small amounts of C).

Before STM measurements, the sample is cleaned by Ar^+ sputtering for 15 min and annealed at the given temperature

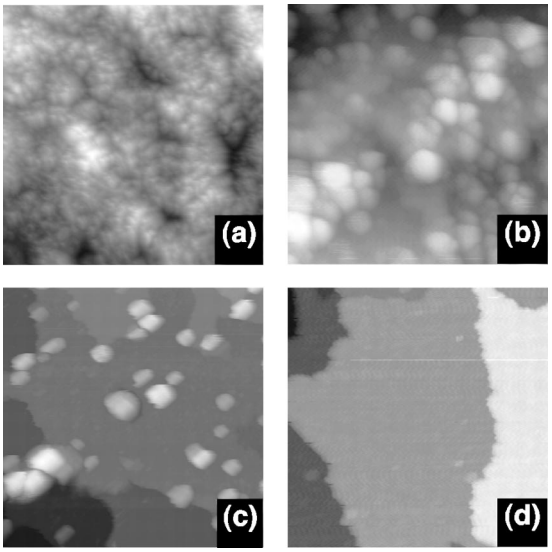

FIG. 1. STM images, taken after annealing at various conditions. The images are measured at 1.0 V and 0.5 nA tunneling current, and are not filtered. (a) After sputtering at room temperature. 1000×1000 Å. (b) After annealing at 700 K. 300×300 Å. (c) After annealing at 800 K. 1000×1000 Å. (d) After annealing at 900 K. 1000×1000 Å.

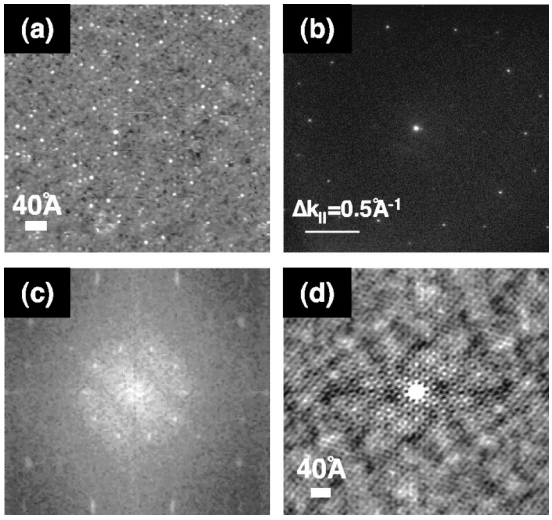

FIG. 2. Large-scale characteristics of the flat terraces obtained after annealing at 900 K. (a) 500 Å×500 Å STM image. The maximum corrugation across the image (the range of the gray scale) is 0.8 Å. (b) High-resolution LEED pattern of a fivefold surface of *i*-Al-Pd-Mn at 94.4 eV. (c) Fourier transform of (a). (d) Autocorrelation function of (a), ±250 Å×±250 Å.

for 2 h. Auger and SPA-LEED are done after STM measurements to ensure surface cleanliness. The tunneling current is typically 0.5 nA at 1 V. Step heights are calibrated against steps on Ag(100), which from the bulk-crystal structure are 2.04 Å. Step heights are measured by using standard Omicron software to level the image, then construct histograms of pixel intensities. The separations between sharp peaks in the histograms then give the step heights.

Our sample is a flat square wafer, approximately $8.5\times8.5\,\mathrm{mm}^2$ in area, and 1.5-mm thick. The bulk composition of our sample is $Al_{71.3}Pd_{19.1}Mn_{9.6}$, as determined by inductively coupled-plasma atomic-emission spectroscopy. The surface normal was oriented to a fivefold axis within 0.2° by x-ray Laue. This sample was previously used for a LEED study in another chamber.[23]

III. EXPERIMENTAL RESULTS

The surface morphology after sputtering is very rough and clusterlike; upon annealing, the clusters coarsen. Other work by us[23,24] and from other groups[25–27] has shown that some or all of this rough structure is due to formation of a cubic overlayer with [110] orientation. Terraces start to appear at about 700 K, but clusters dot the terraces until 900 K, where finally only the large, smooth terraces remain. This evolution is shown in Fig. 1. A similar cluster-to-terrace evolution has been observed by others, both for surfaces prepared by sputter-annealing[11,12] and by fracture.[7] The fine structure present on the terraces after 900 K annealing is shown in Fig. 2(a).

In this paper, we are concerned solely with the large, smooth terraces and their characteristics. At 900 K, the terraces of Fig. 1(d) are typical of the entire surface, based upon a random sampling with STM. We see three step heights: 6.5 ± 0.2, 4.1 ± 0.2, and $2.4+0.2$ Å. The number of steps used to reach the first and last average value was 72, and 24, respectively. The middle value 4.1 Å, was observed only a few times and was associated with very small terraces. The first two step heights were reported previously by Schaub *et al.*,[9,10] and the 2.4 Å step is reported here for the first time. (It is just the difference between the other two values).

The rotational symmetry of the surface is probed by low-energy electron diffraction (LEED), which reveals fivefold symmetry.[10,17,28] Figure 2(b) shows a high-resolution pattern, measured in parallel with the STM experiments. At this particular electron energy (wavelength), the pattern appears tenfold but at other energies the fivefold symmetry is clear, e.g., in Ref. 17. Because LEED averages information over an area of at least 1 mm^2, fivefold symmetry must be typical of the surface over a length scale much larger than that probed typically by STM. [Furthermore, as shown by Fig. 2(b), the widths of the diffraction spots are very small—corresponding to a real-space terrace length of about 900 Å. Narrow widths corresponding to terraces of about 400 Å have also been observed using x-ray diffraction.[27,29]]

The rotational symmetry of the surface can be extracted also from STM images, in two ways. One is through its Fourier transform, which shows the tenfold symmetry of Fig. 2(c). Another is through the autocorrelation function (ACF), with the tenfold symmetric result shown in Fig. 2(d). (The ACF is a spatial map of the pair-correlation function.) Each of these transformations always introduces or preserves an inversion center; hence, the tenfold symmetry of each transform indicates fivefold *or* tenfold symmetry in real space. Each transform is consistent with the fivefold symmetry of the LEED pattern, and with the fivefold zone axis of the bulk orientation.

A second issue is the degree of positional order within the STM image. In the ACF in Fig. 2(d), correlation maxima (bright spots) are visible even close to the edges, which indicates a strong spatial correlation extending over distances of at least ±250 Å. Note that Fig. 2(d) is obtained from the

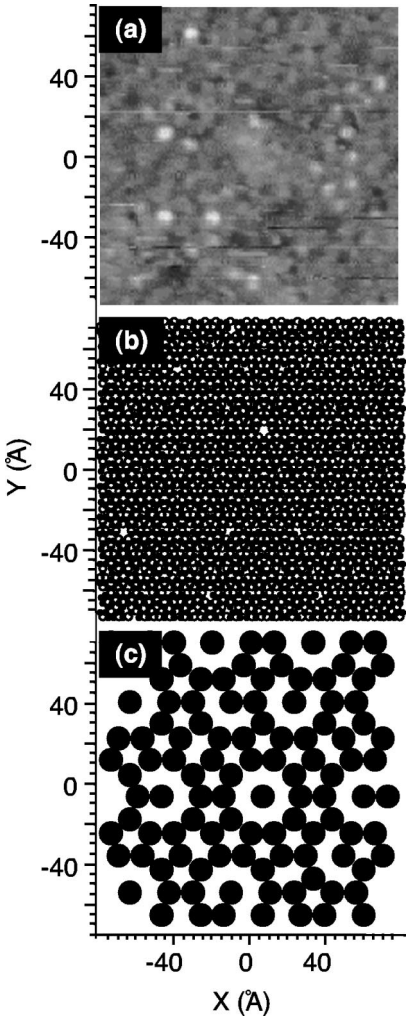

FIG. 3. Possible real-space structures, 150×150 Å images. (a) STM image, a portion of Fig. 2(a). The image has not been filtered. (b) Atomic structure based on the bulk model of Boudard and de Boissieu *et al.* (Refs. 13 and 14) showing one of the terminations favored by LEED I-V analysis (Refs. 17 and 30). The top two planes, separated by 0.38 Å, are shown. (c) Intact PMI clusters, tangent to the topmost plane, shown as black circles.

entire STM image of Fig. 2(a). Similar, albeit noisier, ACF's are obtained if individual features are selected for analysis, e.g., only the white balls or only the black holes in Fig. 2(a). Hence, the STM image actually embodies a high degree of positional order, even though the image appears random upon visual inspection.

The third goal is to identify, if possible, the actual features in the STM image. To that end, we amplify a portion of the STM image in Fig. 3(a), where it can be seen that the smallest features are about 5 Å in diameter, typically larger than the 1–2 Å expected for atomic-scale resolution.

The lateral atomic arrangement expected at a fivefold surface can be deduced by combining certain surface structural analysis with bulk structural information. The surface structural analysis is a full dynamical I-V analysis of the fivefold LEED pattern.[17,30] The IV analysis uses the bulk structure of *i*-Al-Pd-Mn determined from x-ray and neutron diffraction[13,14] as a starting point. The atoms in this model can be assigned to a series of planes. It is natural to use this planar construction for the sputter-annealed surfaces, given that STM shows the terrace corrugation is $\leqslant 1$ Å. However, these planes are not comparable to those in a crystalline structure. No two of them are identical, either chemically or structurally. Furthermore, the interplanar spacings are aperiodic, ranging from several Å to a few tenths of Å.

Among the planes that are perpendicular to the fivefold axis, the best fit between the experimental and theoretical IV curves indicated that the surface is a mixture of similar, relaxed, bulklike terminations.[17,30] These terminations all have a top layer which is 90–100 % Al, and a second layer only 0.38 Å beneath which is about 50% Al and 50% Pd. The two layers are so close that they are appropriately considered a single dense, rumpled layer. (These results of the dynamical LEED analysis are entirely consistent with a more recent study by surface x-ray diffraction.[29]) It should be noted that the IV analysis could not provide exact lateral atomic positions, such as would be provided in an analysis of a typical crystalline surface, because of the lack of lateral periodicity. The atomic positions within the quasicrystalline planes had to be approximated by a type of pair-correlation function that was derived from the bulk structure. The IV analysis confirmed that this was a reasonable approximation, and in addition, was sensitive to atomic compositions in the planes and the interplanar spacings. The lateral atomic positions can be regenerated, however, by returning to the bulk structural model. Using this approach, Fig. 3(b) shows atoms in both of the topmost layers. Visual comparison confirms that the length scale in the STM image is not compatible with the atomic-scale structure. For comparison, in Fig. 3(c) we show also the arrangement of PMI's tangent to the surface of Fig. 3(b). (No intact PMI's are tangent to the second plane in the rumpled layer.) The length scale between PMI's is qualitatively compatible with Fig. 3(a).

Figure 4 shows the ACF's of each real-space structure in Fig. 3. Darker shading means lower probability. Figure 4(a) is the ACF of the STM image of Fig. 3(a); Fig. 4(b) is the ACF of the atomic-scale arrangement shown in Fig. 3(b) (treating all atoms as equal); and Fig. 4(c) is the ACF of the PMI arrangement shown in Fig. 3(c). [Actually, the ACF of PMI clusters—Fig. 4(c)—is the τ^2 inflation of the ACF of the atomic model—Fig. 4(b)]. Visual inspection reveals that each real-space structure produces tenfold symmetry in the ACF. While the features in Fig. 4(b) are much too dense to be compatible with the STM data, the features in Fig. 4(c) have about the same density as the experimental data. This is a graphical confirmation of the fact that the separations between features in the STM image are much too large to reflect the atomic structure.

The comparison is put on a more quantitative basis by constructing histograms of distances between maxima in the ACF's. This is physically equivalent to constructing the radial pair-correlation function. Deriving the histogram from the ACF, rather than from the image itself, serves to reduce the noise in the histogram and assign peak positions more easily. The result is shown in Fig. 5. Figure 5(a) is the histogram of the ACF in Fig. 4(a); Fig. 5(b) is the histogram of the ACF in Fig. 4(b); and Fig. 5(c) is the histogram of the ACF in Fig. 4(c). The histograms of Fig. 5 have not been smoothed or manipulated. They were generated by locating the maxima in the ACF, then calculating the distance between every two such maxima with a 0.2-Å grid. The histo-

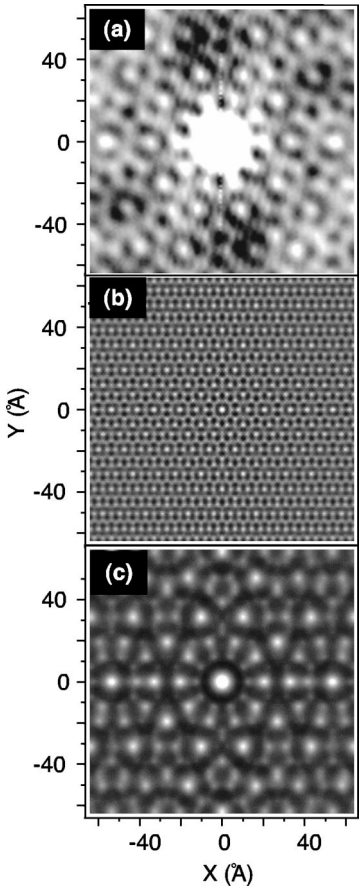

FIG. 4. Auto-correlation functions (ACF's), 128×128 Å. (a) ACF derived from STM of Figs. 2(a) and 3(a). (b) ACF derived from atomic structure model, Fig. 3(b), treating all atoms equally. (c) ACF derived from distribution of tangent PMI's, Fig. 3(c).

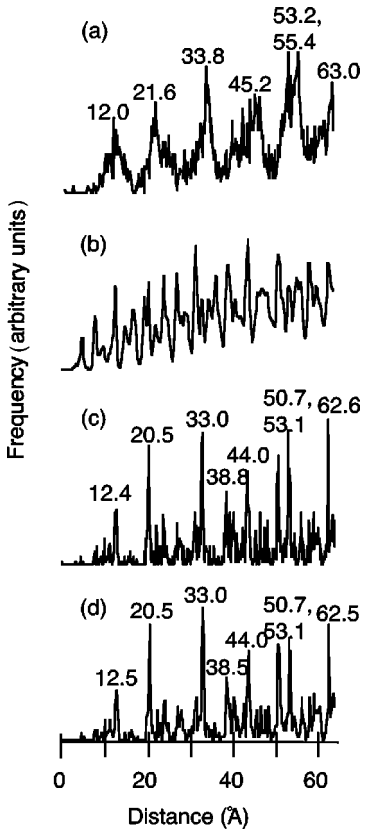

FIG. 5. Histogram of characteristic distances in ACF's. (a) Distances derived from STM of Figs. 2(a) and 3(a). (b) Distances derived from atomic structure model. (c) Distances derived from distribution of tangent PMI's. (d) Distances derived from distribution of broken PMI's.

gram is the frequency of separations between ACF maxima vs distance. The noise in the experimental peak positions adds uncertainty to the assignment of peak positions. Based upon data to be presented later (Table I), the uncertainty due to noise appears to be about 2–3 %. We choose to ignore peaks that are less than about half the intensity of these strong features, since the noise level becomes prohibitive.

The histogram derived from the experimental data [Fig. 5(a)] has distinct maxima at 12.0, 21.6, 33.8, 45.2, 53.2, 55.4, and 63.0 Å. (These are the real maxima, with no smoothing to help determine peak positions.) Clearly, the characteristic separations are not periodic. Furthermore, the most probable separations are the most intense peaks around 34 and 53–55 Å.

For the atomic structure, the characteristic distances, shown in Fig. 5(b), are much smaller, and the peaks are much denser. This provides a quantitative basis for saying that the STM image of Figs. 2(a) and 3(a) cannot show individual atomic features. However, by selecting specific types of atomic *clusters*, the characteristic distances become much larger. The histogram associated with the tangent PMI's is shown in Fig. 5(c). This agrees much better with the STM-derived histogram, Fig. 5(a). The characteristic distances are shown in Table I comparing the experimental values with the values derived from the structural model. Note in Table I that the experimental values are almost all higher than those predicted from the model, by 2.5 to 5 %. This systematic deviation most likely is due to a small miscalibration in the piezoelectrics, which control *xy* motion in the STM. (The feature at 12.0 Å is dominated by a strong spike, presumably noise, which appears to shift this feature anomalously downward.) Assuming that a deviation of 2–3 % is due to instrumental miscalibration, the remaining range of 2–3 % can be attributed to uncertainty in peak positions due to noise.

Hence, it is tempting to say that the STM image shows the electronic environment associated with the intact PMI's. However, we cannot reach quite such a strong conclusion. Some other features are also separated by distances comparable to the PMI clusters, and with comparable probability. The histogram of PMI clusters sliced by the topmost layer [Fig. 5(d)] illustrates this point. Figs. 5(d) and 5(c) are very similar. *Both* agree well with the experimental data of Fig. 5(a), both in the values of the most probable spacings, and in the relative intensities (probabilities). Physically, this is because the broken PMI's cut by the termination shown in Fig. 4(c) are all coplanar; in fact, their histogram is the same as that between intact PMI's tangent to the next-higher termination, 6.6 Å up (based upon the LEED structure analysis[17,30]).

IV. DISCUSSION

STM probes electron density contours. These contours do not necessarily reflect nuclear positions. For this reason,

TABLE I. Characteristic distances. Values in parentheses show the deviation between the experimental value and the value predicted from the PMI model (the unbracketed value in the second column). The bracketed values in the second column show the characteristic separations between Bergman clusters reported by Kasner, *et al.* (Ref. 18).

Distances measured in STM, present work	Distances between PMI's tangent to surface	Distances measured in STM, by Schaub *et al.* (Ref. 9)
12.0 (−3.2%)	12.4 [12.6]	12 (−3.2%)
21.6 (+5.3%)	20.5 [20.3]	19.7 (−3.9%)
33.8 (+2.4%)	33.0 [32.9]	31.7 (−3.9%)
Too weak to be assigned	38.8 [38.6]	36.9 (−4.9%)
45.2 (+2.7%)	44.0 [43.7]	41.3 (−6.1%)
53.2 (+4.9%)	50.7 [50.7]	49.4 (−2.6%)
55.4 (+4.3%)	53.1 [53.2]	51.0 (−4.0%)
63.0 (+1%)	62.6 [62.5]	60.5 (−3.3%)

cases are known where STM does *not* reveal true atomic structure.[31,32] The present paper is one such case. It is always possible, however, that STM will eventually yield atomic resolution on these surfaces, e.g., under different tunneling conditions or with derivatized tips.

Nonetheless, we have shown that the fine structure on the terrace *is* compatible with the bulk quasicrystalline structure, if one selects PMI's or closely-related units as the key structural feature. This suggests that the fine structure probed by STM is really the electronic structure imposed by the PMI's. This is particularly appealing, given that Janot and de Boissieu have argued that the intact PMI's should be extremely stable, and should possess high-local electron density.[15,16] X-ray photoelectron diffraction has indicated that such clusters are present in the surface and near-surface region.[33]

It is possible that common physics—the stability of the PMI's or similar clusters—may underlie the widely different surface topographies presented by the sputter-annealed and fracture surfaces, even though the roughness is an order of magnitude different. Gierer, *et al.*[30] originally realized that the planar surface terminations revealed by the LEED I-V analysis had a high density of intact PMI's. This factor may stabilize these particular terminations *in addition* to the two other factors noted by Gierer *et al.*,[17,30] namely high-Al content and high-atomic density. The flat surface can then be regarded as an array of coplanar PMI's separated by ''filler'' material, which includes broken PMI's.

There are both similarities and differences between our paper and the previous work of Schaub *et al.*,[9,10] who reported terrace fine structure of sputter-annealed fivefold Al-Pd-Mn. For instance, their sample was oriented along a twofold zone axis but formed fivefold facets upon heating to 1025–1075 K, close to the melting point of 1100 K. Our entire surface is fivefold, and is heated to lower temperature, 900 K. Their tunneling currents were typical of a semiconductor (0.05 nA at 2 V), whereas ours are typical of a metal (0.5 nA at 1 V). Their surface exhibited two step heights, whereas ours shows a third. Their STM data showed frequent dark holes separated by a Fibonacci pentagrid; ours does not. These differences suggest that there may be differences between physical characteristics of different sputter-annealed surfaces, perhaps depending upon history and composition. Differences have also been noted in the characteristics of annealed fracture surfaces, and attributed to slight deviations in composition even within a single sample.[7]

However, there are also similarities that point toward the robustness of the major observations in this and in the previous work. Schaub *et al.*,[9] reported ACF's and characteristic distances in good agreement with our own. Their distances are shown in the third column of Table I. It appears that their values also suffered a systematic deviation of a few percent from the ideal, although in the opposite direction from ours—our values being too large, theirs too small. This can probably also be attributed to slight miscalibration in their STM. (Also, it should be noted that their ACF was derived from the dark holes only. Our ACF encompasses all features.) Because Schaub *et al.* reported their distances only as tabulated values, it is not possible to compare relative frequencies of separations, which would also be informative.

Our paper goes further in analyzing the STM-derived data, by comparing with a specific structural model and pointing toward a plausible physical origin. However, alternative interpretations or constructions of bulk structural models exist for *i*-Al-Pd-Mn and similar alloys. The major existing models[13,14,21,34] have strong similarities, notably similarly shaped atomic surfaces in six-dimensional space. Thus, the three-dimensional atomic coordinates are also very similar, although the arrangements of PMI's are rather sensitive to the details of the six-dimensional models.[35] Therefore, some authors stress the importance of the Bergman cluster as a more robust structural motif.[21]

Recently, Papadopolos *et al.* have compared the characteristic distances measured by Schaub *et al.* with arrangements of the Bergman clusters beneath one particular plane.[18,19] The characteristic distances separating Bergman clusters buried beneath this particular plane are shown by the values in brackets in the middle column of Table I. They were calculated from an exact geometrical construction. It can be seen that these distances are virtually identical to the separations between PMI's in our paper, suggesting that both models are consistent with the experimental data.

There is also a proposal that sputter-annealed surfaces might deviate rather subtly from the icosahedral structure, and still exhibit apparent fivefold symmetry, e.g., by adopting two-dimensional quasicrystallinity (pentagonal symmetry) rather than three-dimensional quasicrystallinity (icosahe-

dral symmetry).[5] It is not possible to compare this alternative with STM data as we have done here, because the pentagonal phase is not even known to exist in the bulk, making an extended set of atomic coordinates unavailable for testing. Hence, we cannot use the existing data to address the issue of whether sputter-annealed surfaces of these icosahedral alloys are large unit-cell approximants to the icosahedral phase or not.

In summary, we have analyzed the terrace fine structure revealed by STM for the fivefold surface of *i*-Al-Pd-Mn prepared by sputtering and annealing in ultrahigh vacuum. Even though the image lacks order upon visual inspection, the fine structure is compatible with fivefold symmetry, and shows long-range positional order. Separations between similar features are not periodic, in agreement with expectation for a quasicrystal. The characteristic separations do not correspond to single atoms, but rather to atomic clusters. This shows that the terrace fine structure imaged with STM is electronic in origin. A plausible candidate for the origin of the atomic clusters is the PMI, which is present in the bulk structural model of Boudard, de Boissieu, and coworkers,[13,14] although broken PMI's and buried Bergman clusters[18,19] are also compatible.

ACKNOWLEDGMENTS

M. Quiquandon, Ph. Ebert, A. Goldman, V. Elser, and J. M. Dubois provided valuable comments and suggestions. We thank M. de Boissieu for supplying information about the atomic planes in AlPdMn as well as the software used to generate the three-dimensional atomic bulk positions. This work was supported by the Director, Office of Science, Office of Basic Energy Sciences, Materials Sciences Division, of the U.S. Department of Energy under Contract No. W-405-Eng-82.

[1] D. Shechtman, I. Blech, D. Gratias, and J. W. Cahn, Phys. Rev. Lett. **53**, 1951 (1984).

[2] P. W. Stephens and A. I. Goldman, Sci. Am. **264** (4), 24 (1991).

[3] C. Janot, *Quasicrystals: A Primer*, edited by C. J. Humphreys, P. B. Hirsch, N. F. Mott, and R. J. Brook, Monographs on the Physics and Chemistry of Materials Vol. 48 (Clarendon, Oxford, 1992).

[4] Quasicrystals, edited by D. J. Sordelet and J. M. Dubois [MRS Bull. **22**, (1997)].

[5] J. M. Dubois, in *An Introduction to Structure, Physical Properties and Application of Quasicrystalline Alloys*, edited by J.-B. Suck, M. Schreiber, and P. Hausler (Springer-Verlag, Berlin, 1998).

[6] P. Ebert, M. Feuerbacher, N. Tamura, M. Wollgarten, and K. Urban, Phys. Rev. Lett. **77**, 3827 (1996).

[7] P. Ebert, F. Yue, and K. Urban, Phys. Rev. B **57**, 2821 (1998).

[8] C. J. Jenks, P. J. Pinhero, Z. Shen, T. A. Lograsso, D. W. Delaney, T. E. Bloomer, S.-L. Chang, C.-M. Zhang, J. W. Anderegg, A. H. M. Z. Islam, A. I. Goldman, and P. A. Thiel, in *Proceedings of the 6th International Conference on Quasicrystals (ICQ6)*, edited by S. Takeuchi and T. Fujiwara (World Scientific, Singapore, 1998), pp. 741–748.

[9] T. M. Schaub, D. E. Bürgler, H.-J. Güntherodt, and J. B. Suck, Phys. Rev. Lett. **73**, 1255 (1994).

[10] T. M. Schaub, D. E. Bürgler, H.-J. Güntherodt, J. B. Suck, and M. Audier, Appl. Phys. A: Mater. Sci. Process. **61**, 491 (1995).

[11] J. Ledieu, A. Munz, T. Parker, R. McGrath, R. D. Diehl, D. W. Delaney, and T. A. Lograsso, Surf Sci. **433/435**, 665 (1999).

[12] J. Ledieu, A. W. Munz, T. M. Parker, R. McGrath, R. D. Diehl, D. W. Delaney, and T. A. Lograsso, in *Quasicrystals*, edited by J. M. Dubois, P. A. Thiel, A.-P. Tsai, and K. Urban, MRS Symposia Proceedings No. 553 (Materials Research Society, Warrendale, PA, 1999), pp. 237–242.

[13] M. Boudard, M. de Boissieu, C. Janot, G. Heger, C. Beeli, H.-U. Nissen, H. Vincent, R. Ibberson, M. Audier, and J. M. Dubois, J. Phys.: Condens. Matter **4**, 10 149 (1992).

[14] M. de Boissieu, P. W. Stephens, M. Boudard, and C. Janot, J. Phys.: Condens. Matter **6**, 363 (1994).

[15] C. Janot and M. de Boissieu, Phys. Rev. Lett. **72**, 1674 (1994).

[16] C. Janot, Phys. Rev. B **53**, 181 (1996).

[17] M. Gierer, M. A. Van Hove, A. I. Goldman, Z. Shen, S.-L. Chang, C. J. Jenks, C.-M. Zhang, and P. A. Thiel, Phys. Rev. Lett. **78**, 467 (1997).

[18] G. Kasner, Z. Papadopolos, P. Kramer, and D. E. Bürgler, Phys. Rev. B **60**, 3899 (1999).

[19] Z. Papadopolos, P. Kramer, G. Kasner, and D. E. Bürgler, in *Quasicrystals* (Ref. 12), pp. 231–236.

[20] V. Elser, in *Proceedings of the 6th International Conference on Quasicrystals (ICQ6)* (Ref. 8), pp. 19–26.

[21] V. Elser, Philos. Mag. B **73**, 641 (1996).

[22] Z. Shen, P. J. Pinhero, T. A. Lograsso, D. W. Delaney, C. J. Jenks, and P. A. Thiel, Surf. Sci. **385**, L923 (1997).

[23] Z. Shen, M. J. Kramer, C. J. Jenks, A. I. Goldman, T. Lograsso, D. Delaney, M. Heinzig, W. Raberg, and P. A. Thiel, Phys. Rev. B **58**, 9961 (1998).

[24] F. Shi, Z. Shen, D. W. Delaney, A. I. Goldman, C. J. Jenks, M. J. Kramer, T. Lograsso, P. A. Thiel, and M. A. Van Hove, Surf. Sci. **411**, 86 (1998).

[25] B. Bolliger, M. Erbudak, D. D. Vvedensky, M. Zurkirch, and A. R. Kortan, Phys. Rev. Lett. **80**, 5369 (1998).

[26] D. Naumovic, P. Aebi, L. Schlapbach, C. Beeli, T. A. Lograsso, and D. W. Delaney, in *Proceedings of the 6th International Conference on Quasicrystals (ICQ6)* (Ref. 8), pp. 749–756.

[27] G. Cappello, A. Dchelette, F. Schmithüsen, J. Chevrier, F. Comin, A. Stierle, V. Formoso, M. De Boissieu, T. Lograsso, C. Jenks, and D. Delaney, in *Quasicrystals* (Ref. 12), p. 243.

[28] T. M. Schaub, D. E. Bürgler, H.-J. Güntherodt, J. B. Suck, and M. Audier, in *Proceedings of the 5th International Conference on Quasicrystals (ICQ5)*, edited by C. Janot, and R. Mosseri (World Scientific, Singapore, 1995), pp. 132–138.

[29] M. J. Capitan, J. Alvarez, J. L. Joulaud, and Y. Calvayrac, Surf. Sci. **423**, L251 (1999).

[30] M. Gierer, M. A. Van Hove, A. I. Goldman, Z. Shen, S.-L. Chang, P. J. Pinhero, C. J. Jenks, J. W. Anderegg, C.-M. Zhang, and P. A. Thiel, Phys. Rev. B **57**, 7628 (1998).

[31] Y. G. Ding, C. T. Chan, and K. M. Ho, Phys. Rev. Lett. **67**, 1454 (1991).

[32] P. Sautet, J. Dunphy, D. F. Ogletree, and M. Salmeron, Surf. Sci.

295, 347 (1993).
[33] D. Naumovic, P. Aebi, L. Schlapbach, and C. Beeli, in *New Horizons in Quasicrystals: Research and Applications*, edited by A. I. Goldman, D. J. Sordelet, P. A. Thiel, and J. M. Dubois (World Scientific, Singapore, 1997), pp. 86–94.
[34] A. Katz and D. Gratias, in *Proceedings of the 5th International Conference on Quasicrystals (ICQ5)* (Ref. 28), pp. 164–167.
[35] M. Quiquandon (private communication).